# Biodegradable polyurethane composite scaffolds containing Bioglass® for bone tissue engineering

Joanna L. Ryszkowska, Monika Auguścik, Ann Sheikh, Aldo R. Boccaccini


# Biodegradable polyurethane composite scaffolds containing Bioglass® for bone tissue engineering

Joanna L. Ryszkowska, Monika Auguścik, Ann Sheikh, Aldo R. Boccaccini

PII: S0266-3538(10)00185-5
DOI: 10.1016/j.compscitech.2010.05.011
Reference: CSTE 4716

To appear in: *Composites Science and Technology*

Received Date: 29 December 2009
Revised Date: 1 May 2010
Accepted Date: 5 May 2010

Please cite this article as: Ryszkowska, J.L., Auguścik, M., Sheikh, A., Boccaccini, A.R., Biodegradable polyurethane composite scaffolds containing Bioglass® for bone tissue engineering, *Composites Science and Technology* (2010), doi: 10.1016/j.compscitech.2010.05.011

# Biodegradable polyurethane composite scaffolds containing Bioglass® for bone tissue engineering

Joanna L. Ryszkowska [a *], Monika Auguścik [a], Ann Sheikh[b], Aldo R. Boccaccini [b, c *]

[a] Faculty of Materials Science and Engineering, Warsaw University of Technology, 02-507 Warsaw, Wołoska 141

[b] Department of Materials, Imperial College London, Prince Consort Road, London SW7 2BP, UK

[c] Institute of Biomaterials, Department of Materials Science and Engineering, University of Erlangen-Nuremberg, 91058 Erlangen, Germany

* Corresponding authors. jrysz@meil.pw.edu.pl (Joanna Ryszkowska)

aldo.boccaccini@ww.uni-erlangen.de (Aldo R. Boccaccini)

## Abstract

Five types of solid and porous polyurethane composites containing 5 to 20 wt% of Bioglass® inclusions were synthesized. Porous structures were fabricated by polymer coagulation combined with the salt particle leaching method. In vitro bioactivity tests in simulated body fluid (SBF) were carried out and the marker of bioactivity, e.g. formation of surface hydroxyapatite or calcium phosphate layers upon immersion in SBF, was investigated. The chemical and physical properties of the solid and porous composites before and after immersion in SBF were evaluated using different techniques: Fourier Transform Infrared Spectroscopy (FTIR), Differential Scanning Calorimetry (DSC), Dynamic Mechanical Analysis (DMA) and Thermogravimetric analysis (TGA). Moreover the surface structure and microstructure of the composites was characterized by Atomic Force Microscopy (AFM) and scanning electron microscopy (SEM), respectively. Mercury intrusion porosimetry, SEM and microtomography (μCT) were used to determine pore size distribution and porosity. The fabricated foams exhibited porosity > 70% with open pores of 100 – 400μm in size and pore walls containing numerous micropores of < 10μm. This pore structure satisfies the requirements for bone

tissue engineering applications. The effects of Bioglass® addition on microstructure, mechanical properties and bioactivity of polyurethane scaffolds were evaluated. It was found that composite foams showed a higher storage modulus than neat polyurethane foams. The high bioactivity of composite scaffolds was confirmed by the rapid formation of hydroxyapatite on the foam surfaces upon immersion in SBF.

**KEYWORDS: A. Particle reinforced composites; A. Polyurethane; B. Mechanical properties; B. Porosity/Voids**

## 1. Introduction

Synthetic biodegradable polymers are popular for clinical and surgical applications as it is possible to control their mechanical properties and degradation rates depending on the particular application [1]. These polymers are especially considered in tissue engineering strategies due to their potential ability to enable cell adhesion, migration, proliferation and differentiation [2, 3]. Furthermore synthetic polymers may be processed into a variety of porous structures, using processes such as porogen leaching, rapid-prototyping, electrospinning, thermally induced phase separation, freeze drying, phase inversion and solvent casting [4-10]. However, scaffolds made from synthetic polymers do not exhibit adequate mechanical properties and bioactive behaviour which is a disadvantage for bone tissue engineering applications [10]. One of the ways suggested to improve polymer scaffolds' properties and performance for bone tissue engineering is the development of biodegradable polymer/ bioactive ceramic composites [10, 11]. Hydroxyapatite (HA), bioactive glasses (e.g. Bioglass®) and apatite-wollastonite glass-ceramics are good examples of bioactive inorganic materials suitable for use as fillers in biodegradable polymers [10, 11]. Bioactive glasses have some advantages over other bioceramics, such as excellent osteoconductivity and bioactivity, controllable biodegradability and ability to induce osteogenesis and angiogenesis [12, 13].

Bioglass® of type 45S5 is a member of the family of silicate bioactive glasses [12]. It has been shown that this glass composition especially provides an ideal environment for cell colonization and proliferation, enhancing differentiation of human osteoblasts to form new bone [13]. Bioglass® is bioactive, biocompatible, osteoconductive, nontoxic and noninflammatory as well as being a nonimmunogenic agent. These properties make Bioglass® an ideal filler in biopolymer composite scaffolds as it can be used to improve the mechanical properties of the composites as well as to enhance bioactivity and to influence the scaffold rate of degradation [10, 14,15].

Porous polymer-bioceramic composites for tissue engineering scaffolds have been extensively investigated, as reviewed elsewhere [10]. Composites with Bioglass® inclusions have been produced with different biodegradable polymers, such as PLGA [14], PLLA [16] and PDLLA [15-18].

Degradable polyurethanes have been suggested to manufacture scaffolds for bone tissue engineering [19-23], however very little work has been carried out on developing polyurethane/Bioglass® composites [24].

Polyurethanes (PURs) have tailored elastic properties, thermoplasticity and durability[23]. These properties of PURs are attributed to soft segments that mainly consist of polyester chains and hard segments that are primarily composed of polyurethane blocks [25]. The main characteristics of PURs depend on the microdomain structure of these polymer segments. The structure of PURs, in turn, plays an important role in obtaining good mechanical properties and it affects the ability of the material to be processed into various shapes. PURs have been used for fabricating biomedical devices such as cardiovascular catheters, diaphragms of blood pumps, coating materials for implantable pacemakers and other biomedical products [25]. It is expected that the properties of biodegradable polyurethane elastomers can be adjusted for new applications requiring the use of flexible elastic biodegradable materials in soft and hard tissue engineering.

In general terms, polyurethanes are created by the reaction of a polyol with diisocyanates followed by a chain extension with a diol. As a rule, polyurethanes are formed on aromatic isocyanates characterised by a lack of biocompatibility due to the toxic degradation products released from the aromatic hard segments [26-29]. In order to obtain high level of cell growth and differentiation, the application of aliphatic diisocyanates is preferred over conventional aromatic diisocyanates [30]. Poly(ε-caprolactone) diol is commonly used as a soft segment [31], due to its biocompatibility, enzymatic degradation and slow hydrolytical properties [32]. In our previous investigations conducted on the production of polyurethanes for fabricating porous scaffolds, an aliphatic isocyanate and poly(ε-caprolactone) diol were used [33-36]. In this process poly(ε-caprolactone) urethane elastomers are formed from liquid components in a two-step prepolymer process [33 - 37].

For applications in bone tissue engineering, scaffolds obtained from poly(ε-caprolactone) urethanes exhibit relatively high elasticity and good biocompatibility however their bioactivity, e.g. ability to bond to bone tissue, is low [24]. Thus development of composites with inorganic bioactive fillers is a convenient alternative. The combination of PURs and bioactive glass to produce bioactive composite scaffolds for bone tissue engineering has not been explored in the past, with the exception of our previous investigation of Bioglass® coated PUR foams [24].

In the present investigation, for the first time, biodegradable PUR/Bioglass® composites are developed for bone tissue engineering scaffolds. The scaffolds were fabricated by a salt leaching/polymer coagulation method. A complete physicochemical, microstructural and mechanical characterisation of the new scaffolds is presented.

## 2. Experimental

### 2.1. Materials

The following reactants were used in the synthesis of PURs: 4,4'-dicyclohexylemethane diisocyanates (HMDI), polycaprolactone diol (PCL diol) with molecular weight 2000 Da and dibutyltin dilaurate (DBTDL) purchased from Aldrich Chemical Co. (Germany). Polyol was dehydrated by mixing under vacuum for two hours at 120$^{o}$C. Ethylene glycol (EG) POCH (Gliwice, Poland) was dried under a molecular sieve. The other chemicals were used as received. 1-methyl-2-pyrrolidone was supplied by Fluka, Germany and NaCl granules (crystal size 300-420 μm) were used as a pore former. Bioglass® (grade 45S5) powder (Novamin, Fl., USA) was used as filler. This is a melt-derived bioactive glass powder with mean particle size < 10μm. The composition of 45S5 Bioglass® is: 45wt% $SiO_2$, 24.5wt% $Na_2O$, 24.5 wt% CaO and 6wt% $P_2O_5$, which is the original material developed by Hench et al [12]. This bioactive glass has been extensively used in biomedical applications including tissue engineering [13-18]. To prepare the composites, appropriate quantities of Bioglass® powder were added to the polymer solution to yield composites with different concentrations of Bioglass®.

### 2.2. Polyurethane synthesis

Segmented polyurethanes with molar ratios HMDI/PCL/EG 2:1:1 (A), 2:3:1 (B) and 5:1:4 (C) and constant isocyanates index of 1.00 were synthesized using the two-step polymerisation method. The PCL diol was dried under vacuum for 2 hours at 120$^{o}$C. HMDI and the catalyst were added into the dehydrated PCL diol after cooling from 120$^{o}$C to 60$^{o}$C. The catalyst was added to the polyurethane (A) and (B). The reaction was carried out at 60$^{o}$C for one hour to form prepolymer, then EG was added and mixed for 15 minutes. The reaction was then kept at a temperature of 110$^{o}$C for 8 hours.

### 2.3. Composites synthesis

In a typical production run, appropriate amounts Bioglass® powder were added to the solvent (1-methyl-2-pyrroloidone). Subsequently, the mixture was sonicated for 10 min under 40kHz (VCX-750) (Sonics and Materials Inc.) to improve the dispersion of Bioglass® particles in the polymer matrix.

The mixture was then added and mixed with PCL diol and then the solvent was evaporated. PCL diol and Bioglass® were mixed in selected proportions under vacuum for two hours at a temperature of 120$^{o}$C. The filler was added to the chosen polyurethane matrix at 5wt% and 20wt% proportional to the whole weight of the polymer. Thus five types of composites were produced with matrix type A, labelled: A5 (5 wt% Bioglass®), A10 (10wt% Bioglass®), A20 (20wt% Bioglass®), matrix B with 20wt% of Bioglass® (B20), and matrix C with 20wt% of Bioglass® (C20).

### 2.4. Foam preparation

Porous scaffolds were fabricated by polymer coagulation combined with the salt-particle leaching method. The starting materials (PUR and composite mixtures) were set at liquid nitrogen temperature with a laboratory grinder (Retsch ZM 200, Germany) and dissolved in 1-methyl-2-pyrrolidone at a concentration of 20wt%. The NaCl crystals were fractioned to sizes ranging from 300 to 420µm. The particles were subsequently incorporated into the polyurethane solution with a mass ratio of polymer to NaCl of 1:5. The polymer/salt/solvent mixture was poured into a Teflon mould (6mm in diameter) and immersed in distilled water for 2 days, during which precipitation of the polymer and leaching of the salt particles occurred simultaneously. Water was gently stirred and changed several times in order to increase salt leaching and solvent removal. The obtained porous polyurethane samples, of thickness approximately 6mm, were dried under vacuum at 37$^{o}$C. The obtained bulk and porous polyurethane and composite specimens were sterilized using irradiation dose of 25 kGy.

### 2.5. Assessment of acellular bioactivity in simulated body fluid (SBF)

SBF solution was prepared according to the standard procedure introduced by Kokubo et al [38]. Specimens were immersed in 30ml SBF in clean centrifuge tubes. These were placed inside an incubator at a controlled temperature of 37°C and pH 7.4. Samples were extracted from the SBF solution after given periods of time up to 12 weeks. Once removed from the solution, the samples

were rinsed gently with deionised water and left to dry at ambient temperature in a dessicator prior to further characterisation.

## 2.6. Characterization

### *2.6.1. Fourier transform infrared (FTIR) spectroscopy*

Infrared spectra of PURs were collected using a FTIR spectrophotometer (Thermo Electron Corporation model Nicolet 6700). Measurements were carried out using attenuated total reflectance (ATR) technique. Each sample was scanned 64 times at a resolution of 4$cm^{-1}$ over the frequency range of 4000-400$cm^{-1}$. Analysis of FTIR data enabled to determine the carbonyl hydrogen bonding index (R). The intensities of the carbonyl stretching vibrations of free and hydrogen-bonded groups overlapping bands were located at 1722$cm^{-1}$ and 1694$cm^{-1}$ and analysed. Afterwards, a straight baseline was drawn in the spectrum between 1760$cm^{-1}$ and 1640$cm^{-1}$ and the carbonyl stretching zone was corrected by subtracting the baseline. To estimate the signal strengths, peak modelling of the infrared active carbonyl bands was carried out using the Gaussian curve-fitting method in Origin® 6.0 software. The carbonyl absorption bands were deconvoluted absorbance A (after correction), the carbonyl hydrogen-bonding index R was calculated using Eq. 1 [39, 40]:

$$R = \frac{A_{bonded}}{A_{free}} \qquad \textbf{Equation 1}$$

Moreover the degree of phase separation (DPS) was obtained through Eq. 2:

$$DPS = \frac{R}{R+1} \qquad \textbf{Equation 2}$$

### *2.6.2. Differential Scanning Calorimetry*

Differential scanning calorimetry (DSC) measurements were performed with a MDSC Q 1000 (TA Instruments). The sample mass for these measurements was in the range 9-11 mg. Samples were encapsulated in standard aluminium pans and all tests were carried out under inert nitrogen. The

samples were heated/cooled/heated at a heating rate of 10°C $min^{-1}$ between -80°C and 250°C, with oscillation amplitude of 1°C and a period of 40s.

### *2.6.3. Dynamic Mechanical Analysis*

Compression tests by dynamic mechanical analysis (DMA) were carried out on cube shaped specimens with dimensions of 3x3x3$mm^3$. The tests were carried out on a Thermal Instruments dynamic mechanical analyser (Q800 TA). The frequency-dependant storage modulus was also evaluated with a 4.5 to 9Hz frequency sweep at a constant temperature of 37°C with 1.5% strain and 0.01N static force. Similar parameters were used by Hafeman and co-workers [41]. The storage modulus (E') value was recorded as a function of frequency. The value quoted was the arithmetic mean of three measurements (± standard deviation).

### *2.6.4. Thermogravimetric Analysis (TGA)*

The analysis was carried out using samples of 5 mg in alumina crucibles under a heating rate of 10°C/min under $N_2$.

### *2.6.5. Weight loss*

The weight loss of composites during immersion in SBF was calculated using Eq. 3.

$$\Delta m = \frac{m_t - m_0}{m_0} \times 100\% \qquad \textbf{Equation 3}$$

where $m_0$ and $m_t$ are the masses of the specimen before and after t days in SBF immersion, respectively. The values presented are the arithmetic mean of five measurements (± standard deviation).

### *2.6.6. Scanning Electron Microscopy*

The structure of films and foams before and after immersion in SBF were characterized by scanning electron microscopy (SEM) (Hitachi 5500). SEM observations were performed after coating the samples with a thin film of carbon. EDS and SEM analysis were used to verify if hydroxyapatite (HA)

had formed on the surface of the samples treated in SBF, this being the marker of bioactive behaviour [12, 15]. Specimens were cut using a razor blade. The resulting cross-sections were coated in gold under vacuum using an automatic coating sputter which was set at 10mA for 3 min (Polaron SC7640).

### *2.6.7. Mercury intrusion porosimetry*

Mercury intrusion porosimetry (Micromeritics Autopore II 9220) was used to determine pore size distribution and open porosity (Po) of the foams. In this technique, mercury is intruded into pore spaces under high pressure. As mercury intrusion occurs, the cumulative volume of the intruded mercury at each pressure step is recorded on an intrusion curve. Using the Washburn equation pore sizes and volume distribution by pore sizes were calculated [42].

### *2.6.8. Total Porosity (Pt)*

The total porosity of scaffolds was calculated using the following equation:

$$Pt = \left(1 - \frac{q_{scaffold}}{q_{polymer}}\right) \times 100\% \qquad \textbf{Equation 4}$$

where $q_{scaffold}$ is the scaffold density, determined by measuring the dimensions and the mass of the scaffolds, and $q_{polymer}$ is the density of the solid phase (PUR or composite material).

### *2.6.9. Contact angle measurements*

The water contact angle of selected polyurethane samples was measured at room temperature by the sessile drop method using a goniometer PGX (Fibro Systems AB). The values presented are the arithmetic mean of six measurements (± standard deviation).

### *2.6.10. Atomic force microscopy (AFM)*

AFM was performed with a Multimode NanoScope Va (Digital Instruments, Santa Barbara, CA). Topographic images were obtained in Tapping Mode. The microstructure of polyurethane foams was

investigated on micro sections. These were prepared using a rotary microtom RM 2165 (Leica) with a LN 21 cooling device working at -20°C.

#### *2.6.11. Microtomography (μ-CT)*

Samples for μCT were mounted on a dedicated sample holder and the tungsten reflection target of the μ-CT system was set at a voltage of 60kV and a current of 168μA. Radiographs with isotropic resolution of 4.9μm in terms of pixel/voxel size were acquired by means of a CCD camera of 4000 x 2096 pixels binned to 2000 x 1048. A frame averaging of 3 and a rotation step of 0.4° between individual radiographs, covering a view of 180°C, were chosen. The projections were processed using a modified Feldkamp cone-beam algorithm and a stack of 2D cross section images of the samples were obtained [43]. The data were analyzed with the "CTAn" software package in order to create a 3D representation of the initial microstructure of the foams and to calculate the porosity.

## 3. Results

### 3.1. Polyurethane and composite films

The polymers obtained in the study were aliphatic, segmented polyurethanes based on PCL diol. Although the possible toxicity of the degradation products of these PURs was not studied here, previous investigations have confirmed that the lack of toxic products from these PURs. For example, in previous investigations [29, 44-47] on the characteristic of PUR degradation, special attention has been paid to the identification of diamines as possible degradation products. Aromatic diamines, for example, have not been identified as degradation products of PUR manufactured from aromatic diisocyanates [29, 44-47]. Moreover, in the recent complete study by Bil [48], the identification of degradation products of PUR manufactured from 4.4'-dicyclohexylmethane diisocyanates (HMDI), (PCL diol) and (EG), with structure resembling PUR C, was carried out. The degradation study in static conditions during 20 weeks confirmed that 4.4'-dicyclohexylmethane diamine was not a product of PUR's degradation. Moreover degradation products of this PUR did not lead to cytotoxic reactions on live cells in vitro [48].

In the present study, the morphology of the polyurethanes was modified by changing the molar ratio of the substrates. To help the description of the materials it is useful to consider the hard segments (HS) wt% in the polyurethane. This is related to the molar number and the molar masses involved as follows:

$$\%HS = \frac{nM_{HMDI} + mM_{EG}}{nM_{HMDI} + kM_{PCL} + mM_{EG}} \qquad \textbf{Equation 5}$$

where the average molecular weight of the reagents (g/mol) is given by letter M and letters n, m, k denote the mole number of the reagents. The HS content values calculated for the different PUR matrices are: PUR A: 17wt%, PUR B: 22wt% and PUR C: 44%.

**Figure 1**

Typical FTIR spectra of polyurethanes are shown in Figure 1. These spectra reveal the presence of characteristic polyurethane bands, N-H stretching vibration at 3330-3450cm$^{-1}$, asymmetric and symmetric $CH_2$ stretching at 2934cm$^{-1}$ and 2850cm$^{-1}$, respectively, while other modes of $CH_2$ vibrations are manifested by the bands at 1463, 1419, 1396, 1365 and 1295cm$^{-1}$ [49]. Characteristic for urethane are the bands in the range 3330-3450cm$^{-1}$ and the amide I in the range 1722-1690cm$^{-1}$ [50, 51]. The absorption of amide II (urethane N-H bending +C-N stretching) is located at 1522cm$^{-1}$ and amide III is located in the range 1225-1239cm$^{-1}$ [52]. The band from C-O-C of urethane is located at 1039-1044cm$^{-1}$ [53]. Characteristic for the soft segments are bands at 2934cm$^{-1}$, 2850cm$^{-1}$ and in the region 1449-1463cm$^{-1}$. The absorbance at 1164cm$^{-1}$and 1096cm$^{-1}$ was attributed to ester bonds [4], and the C-O-C stretching vibration band is seen at 1039-1044cm$^{-1}$ [53-55].

The amino groups and the carbonyl stretching regions are of special attention due to their particular relevance in the phase separation of segmented polyurethanes. The degree of the microphase

separation of segmented polyurethanes can be determined from the extent of hydrogen bonding in the hard segments. This type of bonding can be monitored by FTIR by detecting the shifts in N-H and C=O stretching frequencies to lower values than those observed when these groups are not hydrogen bonded [50, 55]. The regions for the N-H stretching band are seen in both curves. There are single bands located at 3369cm$^{-1}$ and 3367 cm$^{-1}$ assigned to the hydrogen bonded N-H vibration. The free (non-hydrogen bonded) N-H stretching band appears as a weak shoulder absorbing at ~3340cm$^{-1}$ [56]. This indicates that most of the N-H groups in the obtained polyurethanes were nearly completely hydrogen bonded. The FTIR spectra show the 1760-1600 cm$^{-1}$ region assigned to the urethane and PCL ester C=O group. The carbonyl bands at 1720-1721cm$^{-1}$ and 1732cm$^{-1}$ can be assigned to free urethane and ester, respectively. Moreover, the stretching bands at 1698cm$^{-1}$ and 1701cm$^{-1}$ are due to the absorption of hydrogen bonded C=O of urethane linkages.

IR spectra for the polyurethane C, Bioglass® powder and composite C20 are presented in Figure 2. The spectrum of Bioglass® revealed the presence of characteristic bands, with the peak at 1031cm$^{-1}$ being from the phosphate group ($PO_3^{-4}$).

**Figure 2:**

The spectra of composite C20 revealed the presence of characteristic bands for the polyurethane matrix. The absorbance of peaks characteristic of the composite matrix is seen to decrease. The appearance of the Bioglass® characteristic group is masked by the overlapping band of the polyurethane matrix. A peak is observed at 3500cm$^{-1}$ which may be due to stretching O-H groups. The susceptibility of non-hydrogen bonded urethane to hydrolysis is higher than that of hydrogen bonded urethane groups [57, 58].

AFM was used to characterise the dispersion of Bioglass® particles in the polyurethane matrix considering that phase imaging provides information about surface stiffness variation related to changes in Young's modulus. From AFM images (results not shown here for brevity) it was confirmed that Bioglass® particles are not well bonded the polyurethane matrix. Figure 3 shows SEM

images of fracture surfaces of composites A20 (Figure 3a) and C20 Figure 3b). The images of Bioglass® agglomerates in composites A20 and C20 are different. The agglomerates in composite C20 are smaller and are better infiltrated by the polyurethane matrix. The surface hydrophilicity of selected samples was characterized by static water contact angle measurements. The measured contact angles on polyurethane surfaces are listed in Table 1. The contact angles equal 71$^{o}$ for PUR A and 75$^{o}$ for both PUR B and PUR C. It was also shown that the contact angle decreased with an increase in Bioglass® content. Static contact angle measurements confirmed the hydrophilic nature of the polymer composites. The smallest contact angle (69$^{o}$) indicating the most hydrophilic surface, was measured for composites A20 and B20. It is worth to note that contact angles for all samples are lower than contact angles of polyurethanes used in commercial implantable devices (75-80$^{o}$) and culture grade polystyrene (80-85$^{o}$) [59]. The contact angle values measured on the composites are similar to values determined on related composites made of P(3HB) containing 20wt% Bioglass® [60].

**Figure 3**:

Polyurethanes density depends not only on hard segment content but also on other structural characteristics. For example, the high density of polyurethane can result also from the high crystallinity of soft domains. In this study, the density of PUR C is higher than that of PUR B since PUR C contains more hard segments. However the density of PUR A, containing a small number of hard segments, is the result of crystallization that took place in the soft domains of this polymer. It is also observed that the composites density increased with Bioglass® content, as expected, considering that the density of Bioglass® equals 2.7g/cm$^3$ [12].

### 3.2. Polyurethane and composite foams

Porous polyurethane and composite scaffolds were fabricated by using selected concentrations of grounded materials and solvent and added NaCl particles as porogen fillers. The structure of composites C20 was brittle and foams cracked during fabrication, therefore this composition could

not be used to produce suitable scaffolds for further investigation. PUR A and PUR B scaffolds were seen to exhibit macroporous structure showing interconnected open pore channels, with pore size varying from 100 to 350µm, and interconnected micropores of size 10-90µm. Representative SEM images of the scaffolds are shown in Figure 4. Bioglass® particles are observed on the pore surfaces and also embedded in the walls of the composite scaffolds. The measured pore sizes of pure polyurethane and composite scaffolds are presented in Table 2.

**Figure 4**

The scaffolds present irregular, slightly rounded macropores with smaller pores mostly in the walls. In all the observed scaffolds, the macropores are interconnected and thus in principle the scaffolds are suitable for bone tissue engineering [3, 10, 11]. However, slight differences exist between the five types of scaffolds prepared; the rougher and more irregular structure of scaffold surfaces was observed on scaffolds containing Bioglass® particles, compared to those without Bioglass®. Moreover thicker walls and a more uneven structure were observed on composite scaffolds (Figures 4e- 4l), compared to pure polyurethane scaffolds (Figures 4a – 4d). Nevertheless these qualitative differences are small and difficult to quantify by electron microscopy analysis, however they may prove significant for the biological application of the scaffolds in contact with relevant cells, taking into consideration the significant effects of surface roughness (micro and nanotopography) on cell attachment and proliferation [61].

In polyurethane, soft and hard domains could crystallize and the crystalline phase could influence the material degradation. DSC measurements were used to characterize the effects of Bioglass® content on the organization of macromolecules in the composites. Examples of DSC curves obtained for the porous and bulk specimens are illustrated in Figure 5. The DSC curves display glass transitions of segments (Tg) and sharp melting endotherms (Tm). The DSC results showing also the values of enthalpy of fusion (ΔHm) are summarized in Table 3.

**Figure 5**:

The glass transition temperatures (Tg) of soft segments increased with increasing amount of Bioglass® (Table 3). The DSC curves (Figure 5) demonstrate melting endothermic peaks (Tm) ranging from 43°C to 50°C. Sharp melting endotherms were observed for all samples indicating the microcrystalline structure of PCL soft segments [62]. The melting temperatures of soft segments increased with increasing amount of Bioglass®. Only for composite B5, Tm decreased with Bioglass® content but this composite demonstrated two melting endotherms, a first sharp peak at Tm = 44.1°C and a second wide peak at Tm = 106°C. The enthalpy of fusion decreased for composites A and increased for composites B. This is caused by the restricted mobility of macromolecules due to their interaction with the particle surface and it is also related to the formation of secondary structures [63], which will be discussed in the Section 4.

Table 3 summarises the results of dynamic mechanical tests carried out on scaffolds using frequency sweep tests at 37°C in terms of storage modulus E' (which represents the energy stored elastically). The storage modulus of composites increased with increasing amount of Bioglass®, as expected. For composite A20; E' is 6.5 times higher than for polyurethane A. For composites B5, B10 and B20 the values for E' are 2.8 times, 4.1 times and 4.8 times (respectively) higher than for neat polyurethane B.

### 3.3. Polyurethane and composite foams after degradation in vitro (SBF)

The degradation and bioactivity of scaffolds was investigated in vitro by immersion tests in acellular SBF. Evidence for changes due to soft and hard segment degradation was obtained by the ATR-FTIR spectra of aged specimens. Figure 6 shows the spectra of composites B with 20 wt% Bioglass® inclusions, in as fabricated condition and after 2, 4, 8 and 12 weeks in SBF.

Figure 6:

The peaks at 1292cm$^{-1}$ are from N-H and C-N stretching vibration of amine, and are seen to become weaker with increasing soaking time in SBF. The long carbon chains break into short chains of small molecules resulting in weakening of the C-H stretching vibration of the methyl group at 2927 cm$^{-1}$ .

These results indicate that urethanes degrade via chemical breakage during hydrolysis of urethane bonds; joining hard and soft segments. Regarding the hard segments, preliminary changes in the amide peak intensities at 1522 $cm^{-1}$ (ν(C=N) + δ(N-H)) [64, 65] were observed, indicating hard segment degradation. Simultaneously, urethane hydrolysis weakens the peak at 1725 $cm^{-1}$. The new peak at 3186 $cm^{-1}$ may come from the C-NH groups of hydrolytic biuret [66]. The gradual change in the signal intensity during degradation reflects the changing environment of the carbonyl groups and is characteristic for the number of formed or destroyed hydrogen bonds. The peak height and width of H-bonded and H-free carbonyl decrease with immersion time, becoming smaller for free carbonyl.

Pretsch et al [40] investigated poly(ester urethane) and concluded that FTIR spectroscopy can give clear evidence of significant changes in the degree of phase separation associated with the process of water uptake and hydrolytic ageing. The process of PUR degradation in water is related to the change of degree of phase separation.

The results of FTIR can be correlated with other experimental results, for example analysing degree of phase separation (DPS) data. From the Gaussian peak intensities, the hydrogen bonding index R was calculated according to Equation 1. The increasing R values indicate an increasing participation of carbonyl groups in hydrogen bonding, which is expected to take place in hard segments. Since most of the non hydrogen bonded carbonyl groups can be ascribed to polyester soft segments, the fraction of hydrogen bonded hard segments is a relative measure of the degree of phase separation in PURs. The degree of phase separation and phase mixing was calculated according to Equation 2 and 3, respectively. Typical results on the regular measurement of hydrogen bonding index and the associated degree of phase separation (DPS) and of phase mixing (DPM) are depicted in Figure 7.

The degree of phase separation of neat PUR (and the matrix in the composite scaffolds) decreased after 4 weeks immersion in SBF, however after longer immersion times, it was seen to increase similarly as for the polyurethanes characterized by Pretsh et al [40].

**Figure 7:**

The PUR and composite scaffolds after immersion in SBF showed weaker bonds for PCL at 1242, 1165, 1096 and 1040cm$^{-1}$. The 1165cm$^{-1}$ and 1084cm$^{-1}$ bands were assigned to ester C (O)-O stretching and O-C stretching in the soft segment chains, respectively. The 1040cm$^{-1}$ band assigned to O-C stretching was used as a reference band. The spectrum of the composite B20 after 12 weeks of immersion in SBF showed that the intensities of bands at 1165cm$^{-1}$ and 1084cm$^{-1}$ significantly decreased compared with that of the control sample (before immersion in SBF). The decrease of the above three peaks' intensities after 12 weeks incubation in SBF was attributed to hydrolysis of the ester segments at the specimen's surface and solution interface, which should result in chain scission and dissolution of ester oligomers in the solution [67, 68].

After immersion in SBF for 8 and 12 weeks, the composite specimens showed many new peaks. The 3762cm$^{-1}$ and 3661cm$^{-1}$ bands were assigned to silanol group (Si-OH) stretching. Bands at 3635cm$^{-1}$ have been assigned to OH anti symmetric stretching and 3550cm$^{-1}$ to symmetric OH stretching. Peaks at 3186cm$^{-1}$ relate to $(CO_3)^2$ groups (only after 4 and 8 weeks immersion) [69] and peaks at 2350cm$^{-1}$ relate to $Ca^{2+}$ [70]. The absorption bands of the phosphate group at 603cm$^{-1}$ and 565cm$^{-1}$ [71, 72] together with the absorption bands of the carbonate group at 1448cm$^{-1}$ are characteristic of the FTIR spectra of biologically active hydroxycarbonate apatite. These results indicate the bioactive behaviour of the composite scaffolds, as discussed in detail further below.

The spectra of neat polyurethanes A, B and of their composites with Bioglass® after 12 weeks immersion in SBF were compared. The band at 1448cm$^{-1}$ was present only in the composites' spectra. The presence of the silanol group and ions $Ca^{2+}$, $(PO_4)^3$ and $(CO_3)^2$ was confirmed on the surface of the composite B20. Weak signals at 1514, 1448, 1414 and 870cm$^{-1}$ were observed, indicating the presence of carbonated hydroxyapatite. The band at 1514cm$^{-1}$ is associated with type AB apatite [73]. The bands at 1448, 1414 and 870cm$^{-1}$ are attributed to a partially carbonated type B hydroxyapatite considering that biological apatites are principally of type B [74].

SEM micrographs indicate changes in the surface structure of scaffolds after 12 week of immersion in SBF for polyurethane and composite specimens (Figure 8). For all semicrystalline polymers the amorphous regions are expected to degrade first, producing a rough surface. A crystalline phase of the soft segments of polyurethane, e.g. spherulites of polyurethane A, degraded and produced a rough surface of the pore wall, as shown in Figure 8a. For polyurethane B and all composites, new features of the structure in the form of fine agglomerates appeared on the pore surfaces. Fine particles (~ 300nm in diameter) embedded in the composite surfaces were seen on SEM images. Similar agglomerates were shown in the work carried out by Chen et al [75], who ascribed these formations to the development of hydroxyapatite crystals.

**Figure 8:**

Figure 9:

µCT analysis was performed to quantify the variation of the microstructure of scaffolds before and after immersion in SBF (Figure 9). This technique detected the 3D porosity of both neat PUR and composite foams. The porosity data, reported in Table 4, show that all scaffolds exhibit a high degree of porosity (~50-80 vol. %). The total porosity of polyurethane A and B foams was determined to be approximately 60-65% while the composite porosity was found to be higher. It was also observed that porosity of composites A20, B5 and B10 decreased after soaking in SBF. Moreover µCT data analysis was used to calculate the pore size distribution. The results (not shown here for brevity) for composites A20 and B20 demonstrate that both before and after soaking in SBF the scaffolds exhibit a one modal porous structure, but composites B5 and B10 exhibit a multimodal porous structure. The average pore size reported in Table 4 indicates that the pore size of composite scaffolds was > 100µm. Burg et al [76] have suggested that the optimal pore size for scaffolds for bone tissue engineering should be between 100 and 400µm. For composites A20, B5 and B10 the average pore size decreased after immersion in SBF, only for composites B20 the size of pores increased after immersion in SBF. This behaviour can be understood by considering the bio-erosion

phenomenon occurring during immersion in SBF, in which material bioresorption involves the formation of small pits and micro pores on the scaffold walls. This is also consistent with the scaffold porosity data reported in Table 4, showing that a significant decrease in average pore diameter ($D_1$) occurs after 12 weeks in SBF. In fact, the increase in micropore content, in comparison with the whole porosity, leads to the decrease of the average pore diameter.

The degradation rate of composite B20 is the fastest of all composites investigated; however the thickness of the scaffold walls can increase due to deposition of apatite during SBF immersion. This apatite deposit can also fill the micro pores in the scaffold walls. The deposition of a hydroxyapatite layer on the scaffolds soaked in SBF involves a mechanism of progressive pore clotting, i.e. leading to a decrease in overall porosity. However, the process of PUR degradation should increase porosity and thus the resultant porosity is the sum of the structural changes induced by both processes.

The in vitro degradation profile for polyurethane and composite foams in terms of mass loss was examined (Figure 10). Due to the polycaprolactone based soft block in the neat PUR foams, it was expected that the sample would undergo bulk degradation through hydrolysis of the ester bonds. For this study, rectangular pieces of the porous samples were incubated in SBF at 37$^{o}$C over a 3 month period and samples were collected at weeks 2, 4, 8 and 12.

Figure 10

Figure 10 shows that less than 2% of original mass was eluted from the sample of polyurethane after 4 weeks in SBF. Earlier studies [77] have shown that degradable polyurethane exhibits mass loss to less than 4% of the original mass during the first month of immersion in SBF. The mechanism of degradation however was seen to change after 8 weeks, the mass of the samples increased by 2% during the next 4 weeks. This slow degradation of polyurethanes containing polycaprolactone segments is not unexpected. Polycaprolactone based materials are known to be among the slowest degrading ones in the group of bioresorbable polymers. The mass loss for the composites was seen

to increase with immersion time in SBF and with bioactive glass concentration. The mass loss after 12 weeks in SBF was found to be lower (ten times) for the B20 composites when compared to equivalent P(3HB) 20wt% Bioglass® composites investigated previously [60].

The changes in the structure of polyurethane and composite foams after immersion in SBF were characterised by thermal analysis (DSC and TGA). The data analysis is summarised in Table 3. The glass transition temperatures, melting temperature and enthalpy of fusion of soft segments increased after 12 weeks immersion in SBF. The decrease in molecular weight and the increase in chain mobility of PUR led to low Tg values. It is possible that the increase in the glass transition temperature of polyurethane samples results in physical cross linking of macromolecules after degradation. The connection between macromolecules restricts their mobility and their crystallinity could be lower. However, the enthalpy of fusion of segments of the composite specimen indicated that the crystallinity is in fact higher. There is thus strong indication that Bioglass® particles have restricted the mobility of shorter macromolecules leading to increased Tg, Tm and ΔHm in the composites.

Urethanes are known to be relatively thermally unstable materials and the decomposition temperature of the urethane bond depends on the polyurethane structure. Three mechanisms of decomposition of urethane bonds have been proposed and reactions may proceed simultaneously; (i) dissociation to isocyanates and alcohol, (ii) formation of primary amine and olefin and (iii) formation of secondary amine and carbon dioxide [78-80]. The thermal degradation of polyurethane is characterised by the decomposition of urethane bonds, the degradation of soft segments and the evolution of volatile components. The degradation analysis was carried out using TGA. Several studies [81-83] have suggested that segmented polyurethanes undergo a two stage degradation process. The first stage of degradation (stage-I) between 200 and 370$^{o}$C is a depolymerisation process associated with the urethane hard segments. The second stage (stage-II), between 370 and 500C, is the degradation of the soft segment by polyol depolymerisation. Table 5 lists the

temperature of the peaks, $T_{1max}$ and $T_{2max}$, indicating the temperature that maximised the rates of degradation in stage-I and stage-II. During the first stage of degradation composite specimens are seen to lose 46% weight. The polyurethane matrix contains 22wt% of hard segments, thus indicating that the weight loss is not connected solely with hard segment degradation. The temperature that maximised the rates of thermal degradation of both peaks changed for composite B20 after immersion in SBF (Table 5). The peaks $T_{1max}$ at 293-295$^{o}$C and $T_{2max}$ at 324$^{o}$C disappear after 2 weeks of degradation. Two new peaks appear, $T_{3max}$ at 381-388$^{o}$C and $T_{4max}$ at 396-404$^{o}$C, which weaken with increasing time of immersion in SBF and disappear after 12 weeks. New peaks at 381-388$^{o}$C are due to hard segment degradation. The peak due to hard segment degradation moved to higher temperatures because the degree of phase separation increases and consequently hard segment order and structural stability increase as well. The second new peaks are related to soft segment degradation. It was also confirmed that the polyurethane matrix degraded totally at around 500$^{o}$C.

The mechanical properties of selected B composite foams after 8 weeks of immersion in SBF were evaluated by DMA. The results for the modulus E' after 12 weeks of immersion are presented in Table 3. Figure 11 shows the changes of storage modulus during degradation.

After 8 weeks immersion in SBF; the storage modulus of composites increased, followed by a decrease after 12 weeks. For composites A20, B5, B10 and B20 the storage modulus values are 30%, 4%, 60% and 83% lower, respectively, in comparison with composites before immersion.

**Figure 11:**

## 4. Discussion

Bioresorbable synthetic polymers (such as poly-lactic acid(PLA), poly-glycolic acid (PGA), poly-lactico-glycolic acid co-polymer (PLGA), polyurethane (PUR), polycaprolactone (PCL)) have attracted renewed considerable attention due to their great potential in bone tissue engineering (TE) [3, 7, 10, 11]. In contrast to the majority of the synthetic scaffolds made of PLA, PGA, PLDA and PCL,

poly(urethane) scaffolds can exhibit greater elasticity and a wide range of mechanical properties. This is the result of the variety of chemistries and molecular weights of the various components and of the molar ratios in which they react to form the polyurethane matrix [25].

In this study, aliphatic biodegradable polyurethane elastomers were investigated. The polyurethanes were produced with various molar ratios of components. As a result, polyurethanes containing 17, 22 and 44wt% of hard segments were obtained. The results obtained from Bil et al [36] have indicated that polyurethane containing about 50wt%of hard segments was optimal for the culture of human osteogenic cells.

The bio and cytocompatibilities of polyurethane containing PCL segments have already been extensively reported [84-86]. However polyurethane with PCL segments demonstrates low osteoconductivity compared to various biodegradable polymers. Osteoconductivity is essential for the growth of cells capable of forming bone matrix and ultimately for successful bone ingrowths into scaffolds [10, 11, 15]. As mentioned in the Introduction, bone invasion in scaffolds can potentially be improved and accelerated by the addition of an inorganic osteoconductivity and bioactive component in the polymer [10, 11, 14, 15]. In the present work we used 45S5 Bioglass® [12] to improve the bioactivity and the mechanical properties of the polyurethane foam, forming PUR/Bioglass® composites. This approach follows from previous research on combining Bioglass® with various degradable polymers, as reported in literature [10, 14, 15].

A range of techniques were utilised to fully characterise the new composites. The polyurethanes were synthesised using only hydrophobic polycaprolactone diol, and all materials synthesised had hydrophilic nature. The process of porous structure formation was developed using the same parameters for all materials investigated. As a result different series of foam like scaffolds exhibiting porosity values higher than 70% were obtained, which is adequate for bone tissue engineering applications [10]. The ideal porosity of a scaffold results from a compromise between the scaffold biological and mechanical performances and it depends strongly on the final specific application.

Nevertheless, porosities >70% are usually a requirement [11, 14]. The scaffolds were seen to exhibit macroporous structure with interconnected open pore channels with pore size varying between 100 and 350µm, the interconnected micropores were seen to be smaller than 100µm. It was observed that the foam structure changes with the increase of Bioglass® content. Composites B5 and B10 exhibited heterogeneous microstructure. Probably the pore structure could be improved by using different parameters, e.g. changing the concentration and size distribution of the NaCl grains used as porogen.

Both composites A20 and B20 contain similar Bioglass® additions but different matrix, the comparison of these foams in terms of pore size distribution is presented in Figure 23. It is observed that B20 composite foams have more micropores with diameters lower than ~100µm and more macropores with diameters in the range 100-200µm. The matrix of both composites contained similar amount of hard segments (A20 – 17wt % and B20 – 22wt %) but the crystallinity of the soft domains of the composite matrix was different, i.e. the crystallinity of soft domains in composite A20 was higher. In conclusion, the foam formation process, and hence the final pore structure is influenced by the hard segment content in the composite matrix, degree of crystallinity of the matrix and Bioglass® content.

The composite scaffold were elastic, the glass temperature of soft domains in these composites is lower than -35$^{o}$C. The storage modulus of composites increased considerably (3.0 – 6.5 times) in comparison to pure polyurethane and values in the range 0.48 to 0.81MPa were measured (Table 3).

Gorna and Gogolewski [87] suggest that hydrolysis is the prevalent degradation pathway for in vivo degradation of poly(ester urethanes). Polyurethane hard segments generally degrade slower than soft segments predominantly due to urethane bonds being much less susceptible than ester bonds (of the soft segment) to hydrolytic degradation. Alcohol arises during urethane linkage hydrolysis, amine and carbon dioxide and hydrolysis of ester bond occurs to yield carboxylic acid and alcohol groups [83]. FTIR data analysis indicated that in the investigated materials both hard and soft

segments degraded in SBF. The degree of phase separation indicates that hard segments degraded very slowly. These results are compatible with the presented TGA data.

The intensities of the peak assigned to ester C(O)-O stretching and O-C stretching in the soft segment chains decreased with the increase of immersion time in SBF. This result indicates that the rate of hydrolysis of the ester segment increased. Polyurethane soft segments degraded faster than hard segments, these results are compatible with the TGA and DSC data, as mentioned above. The different pore structures developed during degradation in SBF were documented by SEM observations. For example, SEM micrographs show the changes in the porous structure after 12-week degradation in SBF of polyurethane (Fig. 8) and composites (Fig. 9). For all semicrystalline polymers the amorphous regions are expected to degrade first, producing a rough surface. A crystalline phase of soft segments in polyurethanes can occur as spherulite [63]. It was indicated that both PUR A and PUR B samples contain a crystalline phase with the crystalline content in PUR A being higher than in PUR B which is indicated by the density values (Table 1) and the melting enthalpy of the crystalline phases ($\Delta H_m$- table 3). Polyurethane crystalline phase can form spherulitic structures whose size may change i.a. along with the change in crystalline phase content, use of fillers and conditions of crystallization process [89]. As shown in the SEM micrograph of the PUR A sample, a spherulite structure formed by crystalline phase from soft domains can be seen after degradation (Fig. 8a). The amorphous phase in PUR A sample has degraded and produced a rough surface of the pore wall, as shown in Fig 8a. No such structure is visible in PUR B (Fig 8b).

It is interesting to note that the composites degradation rate in SBF increased with Bioglass® content. Probably the increase of degradation rate is the result of the increase of silanols content on the scaffolds surface. The hydroxide ions from silanols could influence the hydrolysis of the ester bonds and lead to multiple chain hydrolysis depending upon access of hydroxide ions to the polymer chains. In this regard the increase of silanols on the surface of composites B20 after immersion in SBF was confirmed by FTIR data analysis. During immersion in SBF the composite surface revealed a

new structure formed during the various stages of Bioglass® reactions indicating the presence of Si-OH, $Ca^{2+}$, $(PO_4)^3$ and $(CO_3)^2$. Synthetic carbonated hydroxyapatite has been classified as type A or B, depending on the mode of carbonated substitution: $(CO_3)^2$ for OH (type A) or $(CO_3)^2$ for $(PO_4)^3$ (type B). Biological apatites are principally type B [74]. In synthetic powders prepared by wet methods, some fractions of $(PO_4)^3$ as well as OH groups are replaced by $(CO_3)^2$ groups (type AB). In the present measurements, weak signals associated with carbonated type AB apatite and type B hydroxyapatite were found on composite B20 surfaces upon immersion in SBF.

SEM images confirmed the formation of hydroxyapatite. The results indicate that the composites exhibit an initial HA deposition stage followed by gradual increase in HA formation, this result is in agreement with previous studies on SBF immersion of Bioglass® containing composites [10, 14, 15].

The morphology of the formations on the surface of the scaffolds suggests that they are nanocrystalline HA. These formations have a rod like shape with length of about 1.5μm and diameter of 300-350nm. Similar hydroxyapatite whiskers have been investigated by Coreno et al [90].

The results of the microtomography (Table 4) completed the information about the 3D pore structure of scaffolds during degradation in SBF. In the initial stage of degradation, the content of micropores increased. During the second stage, deposition of HA on the surface of the pores, as a result of Bioglass® reactions in SBF, was revealed. The rate of degradation of ester groups caused by the influence of the hydroxide ions from silanols was increased. In the third stage of biodegradation the porosity increased. These results are compatible with the DMA results. After 12 weeks immersion in SBF the storage modulus decreased even by 80% (composite B20) and this decrease is higher with increasing Bioglass® content which is related also to porosity increase.

## 5. Conclusions

Polyurethane/ Bioglass® composite foams of porosity exceeding 70% were fabricated which exhibit open pores of 100 – 400µm in size and pore walls containing numerous micropores (of less than 10µm). This pore structure satisfies the requirements for bone tissue engineering applications. Composite foams showed a higher storage modulus than the pure polyurethane foams, the values being similar to those of composites made with other degradable polymers reported in the literature. The high bioactivity of PUR/Bioglass® composites was confirmed on the basis of the behavior of these materials in SBF leading to the formation of hydroxyapatite on the foams surfaces. Overall, the present PUR/Bioglass® foams represent a novel family of scaffolds with potential applications in bone tissue engineering. However a full evaluation of the cytocompatibilty of the scaffolds and of the effect of Bioglass® additions on osteoblast cell attachment and proliferation has not been carried out yet. In-vitro cell culture studies and In-vivo investigations should be the focus of future studies to continue the scaffolds development.

## 6. References


1. *Hollinger JO, Battistone GC. Biodegradable bone repair materials: synthetic polymers and ceramics. Clin Orthop Relat Res 1986;207:290}305*
2. *Kohn, J.; Abramson, S.; Langer, R. In Biomaterials Sciences An Introduction to Materials in Medicine, 2nd ed,; Ratner, B. D., Hoffman, A. S., Schoen, F. J., Lemons, J. L., Eds.; Elsevier Academic Press: London, 2006; Chapter 2.*
3. *Yang, S.; Leong, K.; Du, Z.; Chua, C., The Design of Scaffolds for Use in Tissue Engineering. Part I. Traditional Factors, Tissue Engineering. December 2001, 7(6): 679-689.*
4. *Guan J, Sacks MS, Beckman EJ, Wagner WR. Synthesis, characterisation, and cytocompatibility of elastomeric, biodegradable poly(ester-urethane)ureas based on poly(caprolactone) and putrescine. J Biomed Mater Res 2002; 61: 493-503.*
5. *Maquet V, Boccaccini AR, Pravata L, Notingher I, Jerome R. Porous poly([alpha]-hydroxyacid)/Bioglass(R) composite scaffolds for bone tissue engineering. I: preparation and in vitro characterisation. Biomaterials 2004;25:4185-4194.*
6. *Athanasiou KA, Korvick D, Schenck RC. Biodegradeable implants for the treatment of osteochondral defects in a goat model. Tissue Eng 1997; 3(4):363}74.*

7. *Ramakrishna S., Mayer J., Wintermantel E., Leong W. Kam, Biomedical applications of polymer – composites materials: a review, Composites Sci. Technology 2001; 6, 1189 – 1224.*
8. *Ishaug SL, Crane-Kruger GM, Yaszemski MJ, Mikos AG. Three dimensional culture of rat calvarial osteoblasts in porous biodegradable polymers. Biomaterials 1998; 19: 1405}12.*
9. *Agrawal CM, Niederauer GG, Micallef DM, Athanasiou KA. The use of PLA}PGA polymers in orthopaedics. In Encyclopedic handbook of biomaterials and bioengineering. New York: Marcel Dekker, 1995. P. 2081-115 (Chapter 30)*
10. *Rezwan K, Chen QZ, Blaker JJ, Boccaccini AR. Biodegradable and bioactive porous polymer/inorganic composite scaffolds for bone tissue engineering. Biomaterials 27(2006) 3413-3431.*
11. *Guarino, V., Causa, F., Ambrosio, L., Bioactive scaffolds for bone and ligament tissue, Expert Rev. Medical Devices 2007;4(3): 405-418.*
12. *Hench LL. Bioceramics. Journal of the American Ceramic Society 1998;81(7):1705 - 1728.*
13. *Xynos, I. D. ; Edgar, A. J.; Buttery, L. D. K.; Hench, L. L.; Polak, M. Gene-expression profiling of human osteoblasts following treatment with the ionic products of Bioglass 45S5 dissolution. J. Biomed. Mater. Res. 2001, 55, 151-157.*
14. *Boccaccini, A. R.; Maquet, V. Bioresorbable and bioactive polymer/Bioglass(R) composites with tailored pore structure for tissue engineering applications, Compos. Sci. Technol. 2003, 63, 2417-2429.*
15. *Roether, J. A.; Boccaccini, A. R.; Hench, L. L.; Maquet, V; Gautier, S.; Je'ro^me, R. Development and in vitro characterisation of novel bioresorbable and bioactive composite materials based on polyactide foams and Bioglass(R) for tissue engineering applications Biomaterials 2002, 23, 3871-3878.*
16. *Lu HH, El-Amin SF, Scott KD, Laurencin CT. Three-dimensional, bioactive, biodegradable, polymer-bioactive glass composite scaffolds with improved mechanical properties support collogen synthesis and mineralization of human osteoblasts-like cells in vitro. J Biomed Res A 2003; 64A: 465-74.*
17. *Zhang K, Wang Y, Hillmayer MA, Francis LF. Processing and properties of porous poly(L-lactide)/bioactive glass composites. Biomaterials 2004; 25: 2489-500.*
18. *Verrier S, Blaker JJ, Maquet V, Hench LL, Boccaccini AR. PDLLA/Bioglass(R) composites for soft-tissue and hard-tissue engineering: an in vitro cell biology assessment. Biomaterials 2004; 25: 3013-21.*

19. *Riboldi SA, Sampaolesi M, Neuenschwander P, Cossu G, Mantero S. Electrospun degradable polyesterurethane membranes: potential scaffolds for skeletal muscle tissue engineering. Biomaterials 2005; 26: 4606-15.*
20. *Guan J, Fujimoto KL, Sacksa MS, Wagner WR Preparationand characterization of highly porous, biodegradable polyurethane scaffolds for soft tissue applications Biomaterials. 2005: 26: 3961-71.*
21. *Riboldi SA, Sampaolesi M, Neuenschwander P, Cossu G, Mantero S. Electrospun degradable polyesterurethane membranes: potential scaffolds for skeletal muscle tissue engineering. Biomaterials 2005; 26: 4606-4615.*
22. *Grad S, Kupesik L, Gorna K, Gogolewski S, Alini M. The use of biodegradable polyurethane scaffolds for cartilage tissue engineering: potential and limitations Biomaterials 2003: 24: 5163-5171.*
23. *Zhang J, Doll BA, Beckman EJ and Hollinger JO. A biodegradable polyurethane ascorbic acid scaffold for bone tissue engineering J. Biomed. Mater. Res. A 2003: 67: 389-400.*
24. *Bil M, Ryszkowska J, Roether JA, Bretcanu O, Boccaccini AR. Bioactivity of polyurethane-based scaffolds coated with Bioglass® particles; Biomed. Mater. 2(2007) 93-101.*
25. *Lamba N.M.K., Woodhouse K.A., Cooper S.L., Polyurethanes in Biomedical Applications, CRC Press, Boca Raton, 1998.*
26. *Marchant RE, Zhao Q, Anderson JM, Hiltner A. Degradation of Poly(ether urethane urea) elastomer: infra-red and XPS studies. Polymer 1987; 28: 2032-9.*
27. *Szycher M, Poirier VL, Dempsey DJ. Development of an aliphatic biomedical-grade polyurethane elastomer. J Elastom Plast 1983; 15: 81-95.*
28. *Pinchuk L. A review of the biostability and carcinogenity of polyurethanes in medicine and the new generation of 'biostable' polyurethanes. J Biomat Sci-Polym E 1994; 6: 225-67.*
29. *Tang YW, Labow RS, Santerre JP. Isolation of methylene dianiline and aqueous- soluble biodegradation products from polycarbonate-polyurethanes. Biomaterials 2003; 24: 2805-19.*
30. *Til HP, Falke HE, Prinsen MK,Willems MI. Acute and subacute toxicity of tyramine, spermidine, spermine, putrescine and cadaverine in rats. Food Chem Toxicol 1997; 35: 337-48.*
31. *Bogdanov B, Toncheva V, Schacht E, Finelli L, Sarti B, Scandola M. Physical properties of poly(ester-urethanes) prepared from different molar mass polycaprolactone-diols. Polymer 199; 40: 3171-82.*

32. *Pitt CG. Poly-e-caprolactone and its copolymers. In: Chasin M, Langer R, editors. Biodegradable polymers as drug delivery systems. New York: Marcel Dekker; 1990. P.71-120.*
33. *Bil M, Ryszkowska J, Sienkiewicz-Latka E, Lewandowska-Szumiel M, Kurzydlowski K. J. Influence of soft domains' size on biocompatibility prepared polyurethanes; The international Journal of Artificial Organs 28 (2005) 4.*
34. *Ryszkowska J, Bil M, Woźniak P, Lewandowska-Szumiel M, Kurzydlowski K. J. Influence of catalyst type on biocompatibility of polyurethanes. Materials Science Forum III, Vols. 514-516, May 2006, 887-891.*
35. *Bil M, Ryszkowska J, Kurzydlowski K. J. Effect of polyurethane composites and the fabrication process on scaffold properties. J Mater Sci (2009) 44: 1469-1476.*
36. *Bil M, Ryszkowska J, Woźniak P, Lewandowska-Szumiel M, Kurzydlowski K. J. Optimization of polyurethane structure as the potential materials for bone tissue engineering, Acta Biomaterialia in press.*
37. *Gorna K, Gololewski S. Biodegradable polyurethane for implants. II. In vitro degradation and calcification of materials from poly(ecaprolactone)-poly(ethylene oxide) diols and various chain extenders. J Biomed Mater Res 2002; 60: 592-606.*
38. *Kokubo T, Kushitani H, Sakka S, Kitsugi T, Yamamuro T. Solutions able to reproduce in vivo surface-structure changes in bioactive glass-ceramic A-W. J Biomed Mater Res 24 (1990) 721-734.*
39. *Tien YI, Wei KH. Hydrogen bonding and mechanical properties in segmented montmorillonite/ polyurethane nano composites of different hard segment ratios. Polymer 2001; 42:3213-21.*
40. *Pretsch T., Jakob I., Müller W., Hydrolytic degradation and functional stability of a segmented shape memory poly(ester urethane), Polymer Degradation and Stability 94 (2009) 61-73.*
41. *Hafeman A. E., Li B., Yoshii T, Zienkiewicz K, Davidson J.M., Guelcher S.A. Injectable Biodegradable Polyurethane Scaffolds with Release of Platelet-derived Growth Factor for Tissue Repair and Regeneration, Pharmaceutical Research, 25 (2008) 2387-2399.*
42. *Ho ST, Hutmacher DW A comparison of micro CT with other techniques used in the characterisation of scaffolds Biomaterials 27(2006) 1362-1376.*
43. *Feldkamp LA, Davis LC, Kress JW, Practical cone-beam algorithm, J Opt Soc Am 1(6) (1984) 612-619.*
44. *Wang GB, Santerre JP, Labow RS. High–performance liquid chromatographic separation and tandem mass spectrometric identification of breakdown products associated with the*

*biological hydrolysis of a biomedical polyurethane. J. Chromatogr. B Biomed. Sci. Appl. 1997;698:69–80.*

45. *Mazzu AL, Smith CP. 1984. Determination of extractable methylene dianiline in thermoplastic* polyurethanes by HPLC. J Biomed Mater Res 18(8):961-968.
46. Amin P., Wille J., Shah K. Kydonieus A., Analysis of the extractive and hydrolytic behavior of microthane poly(ester urethane) foam by high pressure liquid chromatography, J. Biomed Mater Res 27 (1993) 655-666.
47. *Santerre JP, Labow RS, Duguay DG, Erfle D, Adams GA. Biodegradation evaluation of polyether and polyester-urethanes with oxidative and hydrolytic enzymes. J. Biomed. Mater. Res. 1994;28:1187–1199.*
48. *Bil M, PhD Thesis, Polyurethane scaffolds for bone tissue engineering, Warsaw University of Technology, Warsaw 2009.*
49. *Gorna K., Gogolewski S., In vitro degradation of novel medical biodegradable aliphatic polyurethanes based on E-caprolactone and Pluronics® with various hydrophilicities, Polymer Degradation and Stability 75 ~(2002) 113-122.*
50. *Ayres E, Oréfice RL, Yoshida MI., Phase Morphology of hydrolysable polyurethanes derived from aqueous dispersions European Polymer Journal 2007: 43: 9: 3510-3521.*
51. *Chen TK; Tien YI; Wei K, Synthesis and characterization of novel segmented polyurethane/clay nanocomposites, Polymer 41 (2001) 1345-53.*
52. *G Wang, C Zhang, X Guo, Zhiyong Ren, Ftir and molecular mechanics studies of H-bonds in aliphatic polyurethane and polyamide-66 model molecules.*
53. *Mishra A.K., Chattopadhyay D.K., Sreedhar B., Raju K. V. S. N., FTIR and XPS Studies of Polyurethane-Urea-Imide Coatings, Progress in Organic Coatings 2006, 55, 231-243.*
54. *McCarthy SJ, Meijs GF, Mitchell N, Gunatillake P A, Heath G, Brandwood A, Schindhelm K. In vivo degradation of polyurethanes: transmission-FTIR microscopic characterization of polyurethanes sectioned by cryomicrotomy Biomaterials 1997: 18: 1387-1409.*
55. *Irusta I., Fernandez-Berridi M.J., Aromatic poly(ester-urethanes): effect of the polyol molecular weight on the photochemical behaviour, Polymer 41, (2000) 3297-3302.*
56. *Yilgor I, Yilgor E, Guler IG, Ward TC, Wilkes GL. FTIR investigation of the influence of diisocyanate symmetry on the morphology development in model segmented polyurethanes Polymer 2006: 47: 4105-4114.*
57. *Tang YW, Labow RS, Santerre JP. Enzyme induced biodegradation of polycarbonate-polyurethanes: dependence on hard segment chemistry. J Biomed Mater Res, 2001; 57: 597-611.*

58. *Tang YW, Labow RS, Santerre JP. Enzyme induced biodegradation of polycarbonate-polyurethanes: dependence on hard segment chemistry. J Biomed Mater Res, 2001; 56: 516-28..*
59. *Gorna K, Gogolewski S. Molecular stability, mechanical properties surface characteristics and sterility of biodegradable polyurethanes treated with low temperature plasma, Polymer degradation and stability: 2003: 79: 475-485.*
60. *Misra S. K, Mohn D, Brunner TJ, Stark WJ, Philip SE, Roy I, Salih V, Knowles JC,. Boccaccini A, R, Comparison of nanoscale and microscale bioactive glass on the properties of P(3HB)/Bioglass® composites, Biomaterials 29 (2008) 1750-1761.*
61. *Webster, T.J., R.W. Siegel, and R. Bizios, Osteoblast adhesion on nanophase ceramics. Biomaterials, 1999: 20(13): p. 1221-1227.*
62. *Qiu Z, Komura M, Ikehara T, Nishi T. Miscibility and crystallization behaviour of biodegradable blends of two aliphatic polyesters. Poly(butylenes succinate) and Poly(ε-caprolactone) Polymer 2003: 44: 7749-7756.*
63. *Miller G.W., Saunders J.H., The thermal analysis of polymers. II. Thermo mechanical analyses of segmented polyurethane elastomers. J. Applied Polymers Science, 1969, 13(6), 1277-1288.*
64. *Schoonover JR, Thompson DG, Osborn JC, Orler EB, Wrobleski DA, Marsh AL, Wang H, Palmer RA. Infrared linear dichroism study of a hydrolytically degraded poly(ester urethane). Polym Degrad Stab 2001; 74:87-96.*
65. *Schoonover JR, Steckle Jr WP, Cox JD, Johnston CT, Wang Y, Gillikin AM, Palmer RA. Humidity-dependent dynamic infrared linear dichroism study of a poly(ester urethane). Spectrochim Acta, Part A: Mol Biomol Spectrosc A 2007; 67: 208-13.*
66. *Dong Z., Li Y., Zou Q, Degredation and biocompatibility of porous nano-hydroxyapatite/polyurethane composite scaffold for bone tissue engineering. Applied Surface Science 255 (2009) 6087-6091.*
67. *Kim HW, Knowles JC, Kim HE. Effect of biphasic calcium phosphate on drug release and biological and mechanical properties of poly(e-caprolactone) composite membranes. J Biomed Mater Res A 2004; 70: 467-479.*
68. *Verma D, Katti K, Katti D. Experimental investigation of interfaces in hydroxyapatite/polyacrylic acid/polycaprolactone composites using photoacoustic FTIR spectroscopy. J Biomed Mater Res A 2006; 77: 59-66.*
69. *Cairon O., Chevreau T., Lavalley J-C. Brönsted acidity of extra framework debris in steamed Y zeolites from the FTIR study of CO adsorption, J. Chem. Soc., Faraday Trans., 1998, 94, 3039-3047.*

70. *Malek M. A., Chong C. S., FTIR study of H2O in polyallyl diglycol carbonate, Vibrational Spectroscopy, 24, 200, 181-184.*
71. *Wharton D., HickeyL., Frost R. L., Kloprogge J.T., Infrared and Raman study of interlayer anions CO32-, NO3-, SO42- and ClO4- in Mg/Al-hydrotalcite, American Mineralogist, 87, 2002, 623-629.*
72. *Taraschewski, M; Cammenga, HK Tuckermann, R; Bauerecker, S; FTIR study of CO2 and H2O/CO2 nanoparticles and their temporal evolution at 80 K, J Phys Chem A, 109 (2005) 337-43.*
73. *Merry JC, Gibson JR, Best SM, Bonfield W. Synthesis and characterisation of carbonate hydroxyapatite. J Mater Sci Mater Med 1998; 9: 779-83.*
74. *Le Geros RZ. Calcium phosphates in oral biology and medicine. In Myer HM, editor. Monographs in oral science. Basel: Karger; 1991.p. 31.*
75. *Chen Q.-Z. Reswan K., Virginie Franĉon V, Armitage D, Nazhat S.N., Jones F.H., Boccaccini A.R., Acta Biomaterialia 3 (2007) 551-562.*
76. *Burg, KJ, S. Porter, JF Kellam. Biomaterial developments for bone tissue engineering. Biomaterials. 21(23) (2000) 2347-2359.*
77. *Knight P. T., Lee K. M., Qin H., Mather P T. Biodegradable Thermoplastic Polyurethanes Incorporating Polyhedral Oligosilsesquioxane, Biomacromolecules 2008, 9, 2458-2467.*
78. *Van Bogart JWC, Bluemke DA, Cooper SL. Annealing-induced morphological changes in segmented elastomers. Polymer, 22(1981) 1428-38.*
79. *Berta M, Lindsay C, Pans G, Camino G. Effect of chemical structure on combustion and thermal behaviour of polyurethane elastomers layered silicate nanocomposites. Polym Degrad Stab 91 (2005) 1179-91.*
80. *Javni I, Petrovic ZS, Guo A, Fuller R. Thermal stability of polyurethanes based on vegetable oils. J Appl Polym Sci 1999; 77 (8): 1723-34.*
81. *Xu Y, Petrovic Z., Sudipto Das S., Wilkes G.L., Morphology and properties of thermoplastic polyurethanes with dangling chains in ricinoleate- based soft segments, Polymer 49 (2008) 4248-4258.*
82. *Zeng J. B., Li Y-D., Li L-S; Wang Y-Z; Yang K-K, Thermal and thermo-oxidate degradation of poly(ester urethane) containing poly(L-Lactic Acid) and poly(butylenes Succinate) blocks J Macrom. Sci, Part B: Physics 48(2009)635-649.*
83. *Narayan R., Chattopadhyay D. K., Sreedhar B., Raju K. V. S. N., Mallikarjuna N.N., Aminabhavi T. M.; Degradation profiles of polyester-urethane (Hp-MDI) and polyester-melamine (JP-HMMM) coating: A thermal study, J App. Polym. Sci., 97(2005)518-526.*

84. *Saad B, Hirt TD, Welti M, Uhlschmid GK, Neuenschwander P, Suter UW. Development of degradable polyesterurethanes for medical applications: in vitro and in vivo evaluations. J Biomed Mat Res 1997; 36(1): 65-74.*

85. *Henry JA, Burugapalli K, Neuenschwander P, Pandit A. Structural variants of biodegradable polyesterurethane in vivo evoke a cellular and angiogenic response that is dictated by architecture. Acta Biomater 2009; 5 (1): 29-42.*

86. *Grad S, Kupesik L, Gorna K. The use of biodegradable polyurethane scaffolds for cartilage tissue engineering: potential and limitations. Biomaterials 2003; 24: 5163-71.*

87. *Gorna K, Gogolewski S. Biodegradable polyurethanes for implants. II. In vitro degradation and calcification of materials from poly(e caprolactone)- poly(ethylene oxide) diols and various chain extenders. J Biomed Mater Res 2002; 60:592-606.*

88. *Tatai L., Moore T. G. Adhikari R, Malherbe F, Jayasekara R., Griffiths I., Gunatillake G.A, Thermoplastic biodegradable polyurethanes: The effect of chain extender structure on properties and in-vitro degradation, Biomaterials 28(2007) 5407-5417.*

89. *Boczkowska A., Ryszkowska J., Morphology and properties of urea-urethane nanocomposites obtained from crystalline prepolymers with different chemical structure, Solid State Phenomena, Trans Tech Publication (2003) 329-333.*

90. *Coreňo J., Rivera E., Castaňo E, Rogelio Rodrĭguez R., Apatite Growth on Calcium Adsorbed Surface of Wet Flocculated Silica Particles Immersed in a Modified Simulated Body Fluid, Biomed Mater Res (Appl Biomater) 53:44-50, 2000.*

***FIGURE CAPTIONS***

Figure 1: FTIR spectra of polyurethanes A, B and C

Figure 2: FTIR spectra of Bioglass® (B), polyurethane C (C) and composite C20.

Figure 3: SEM images of the surface cross section of composites A20 (a) and C20 (b).

Figure 4: SEM images of porous samples of neat polyurethane PUR A (a, b), PUR B (c, d) and of porous composite samples A20 (e, f), B5 (g, h), B10 (i,j) and B20 (k,l) at different magnifications.

Figure 5: DSC thermograms of porous polyurethane B and composites B5, B10 and B20. The curves have been shifted vertically for clarity.

Figure 6: FTIR of composite B20: as fabricated (1) and after immersion in SBF for 2 weeks (2), 4 weeks (3), 8 weeks (4) and 12 weeks (5).

Figure 7: Hard domain degradation process of composite B5 due to the development of the carbonyl hydrogen bonding index (R), degree of phase separation (DPS) (2) and degree of phase mixing (DPM) (3).

Figure 8: SEM images of the surface (cross section) of porous samples of polyurethane PUR A (a) and PUR B (b) after immersion for 12 weeks in SBF, and of composite B5 after 8 weeks (c) and 12 weeks (d) immersion in SBF.

Figure 9: Micro-computerised tomography analysis of polyurethane B foams before (a) and after (b) immersion in SBF and composites B20 foams before (c) and after (d) immersion in SBF for 12 weeks.

Figure 10: Degradation profile of percentage mass remaining of polyurethane B and composite scaffolds B5, B10 and B20.

Figure 11: Storage modulus as a function of strain rate (compression) during DMA (at 4.5 Hz before) for composite foams after 0, 8 and 12 weeks immersion in SBF.

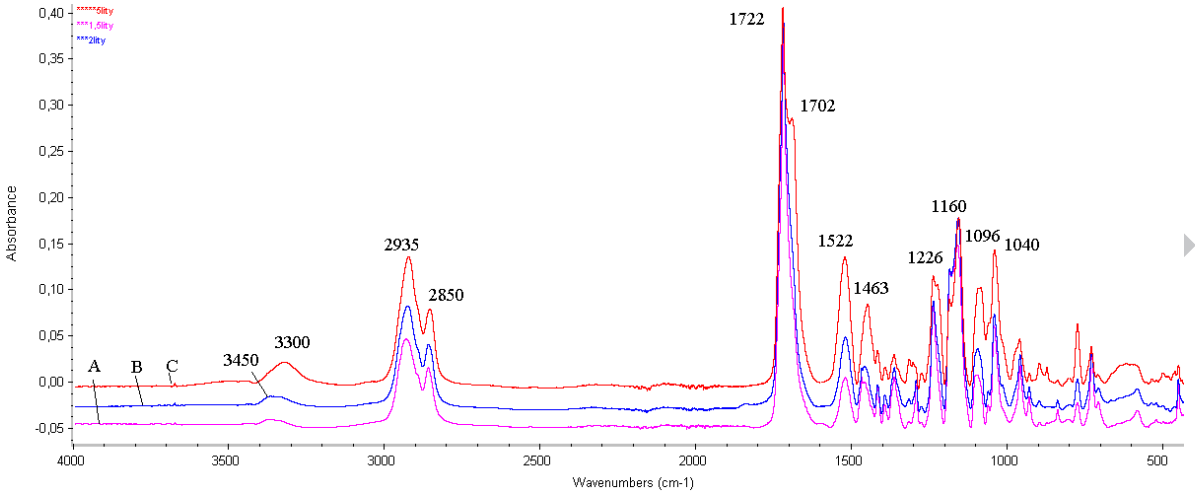


Figure 1

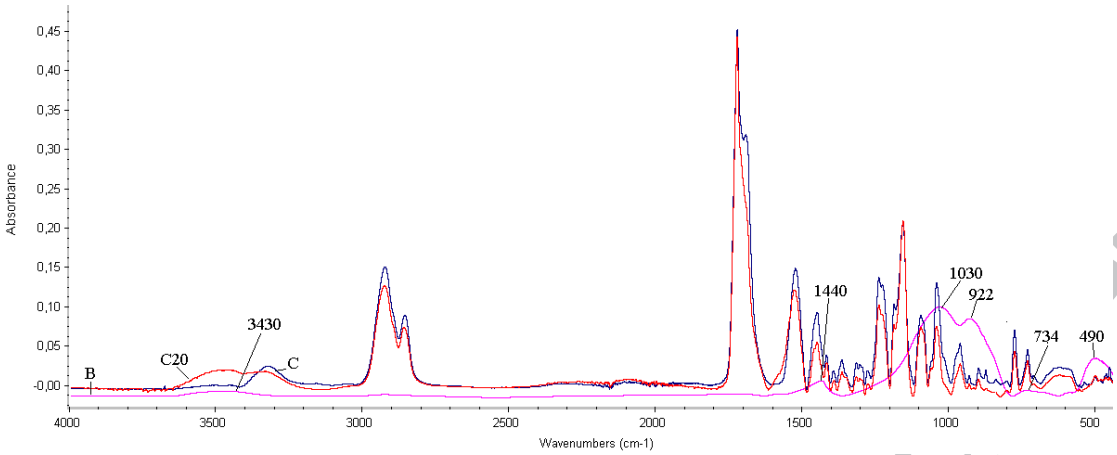


Figure 2

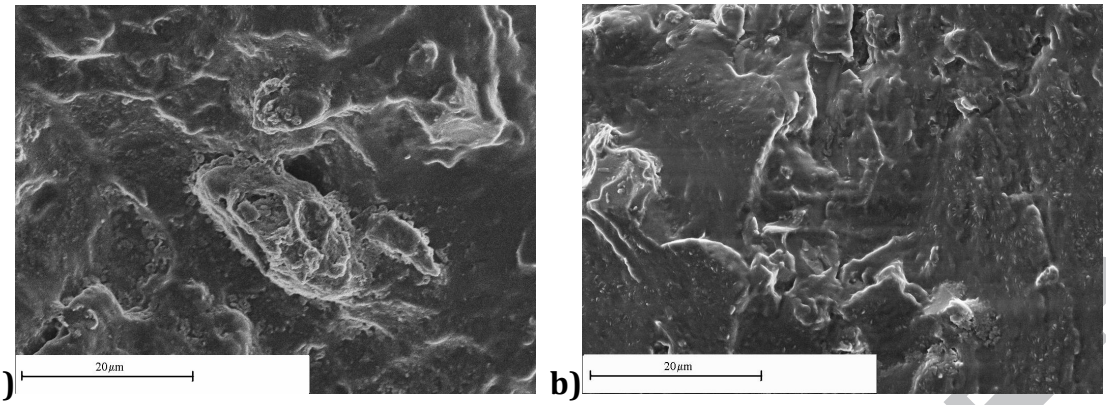


Figure 3

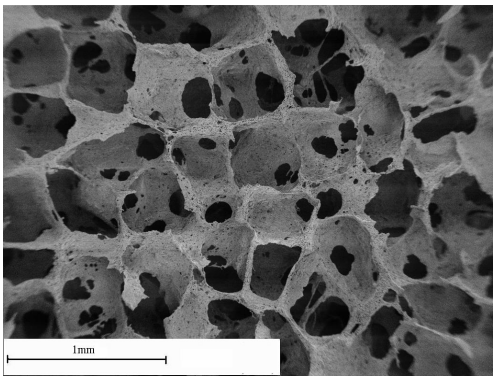


a)

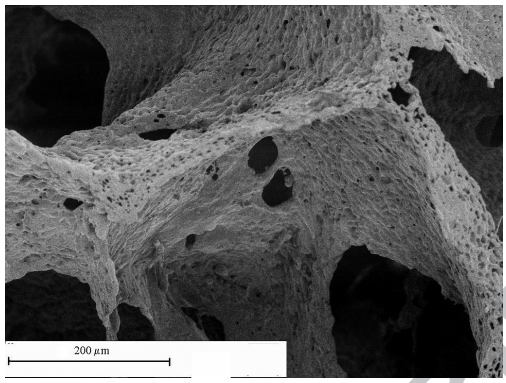


b)

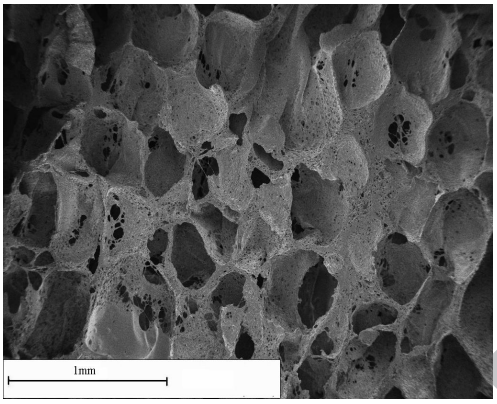


c)

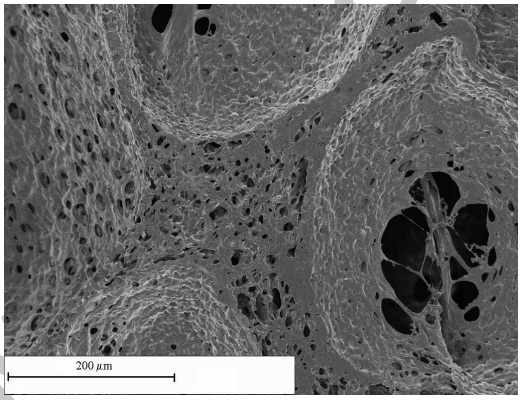


d)

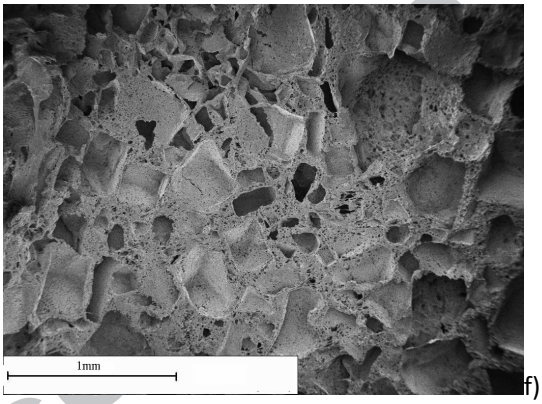


e)

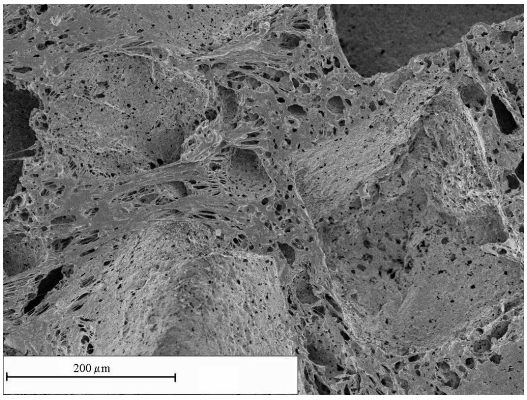


f)

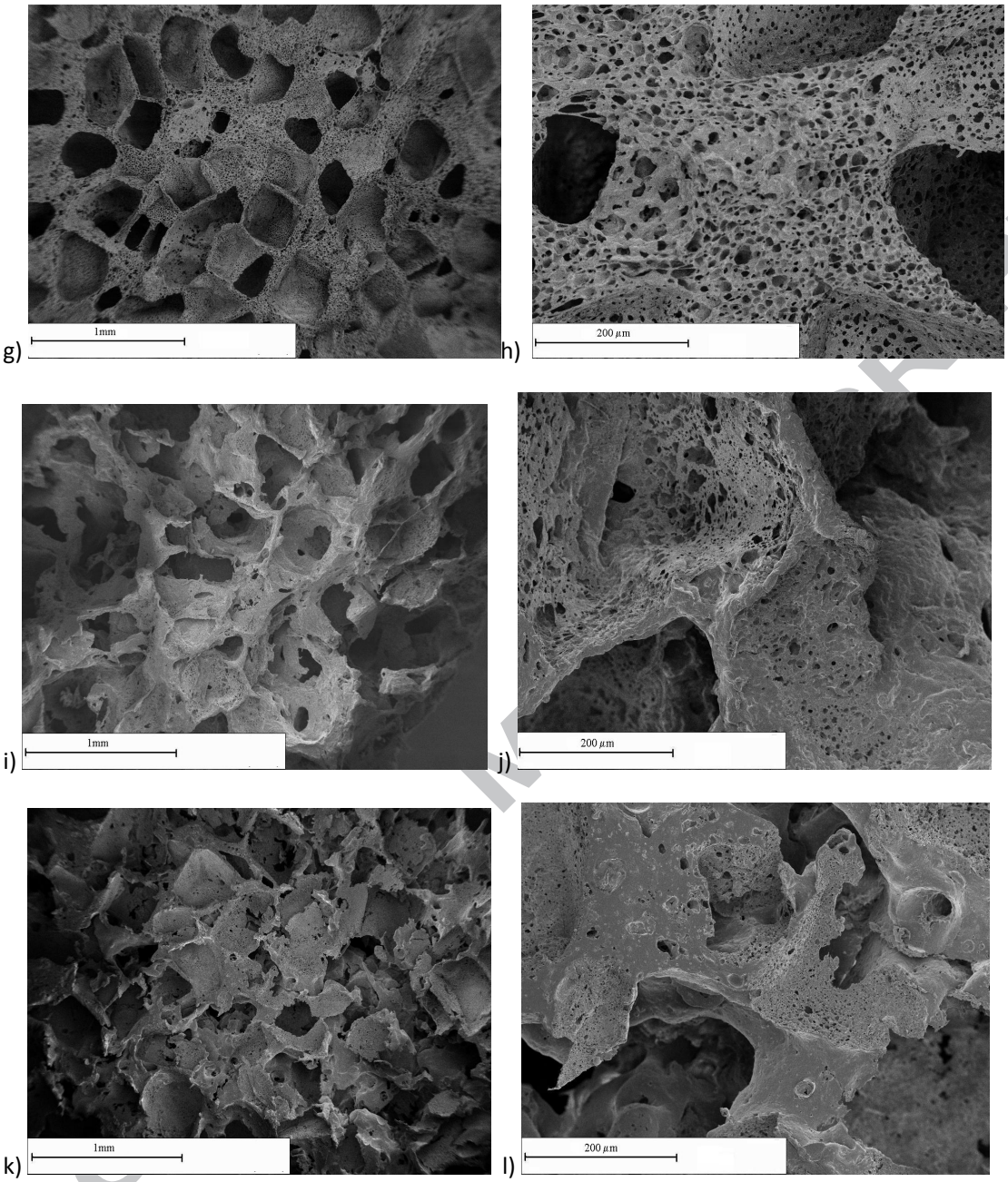


Figure 4

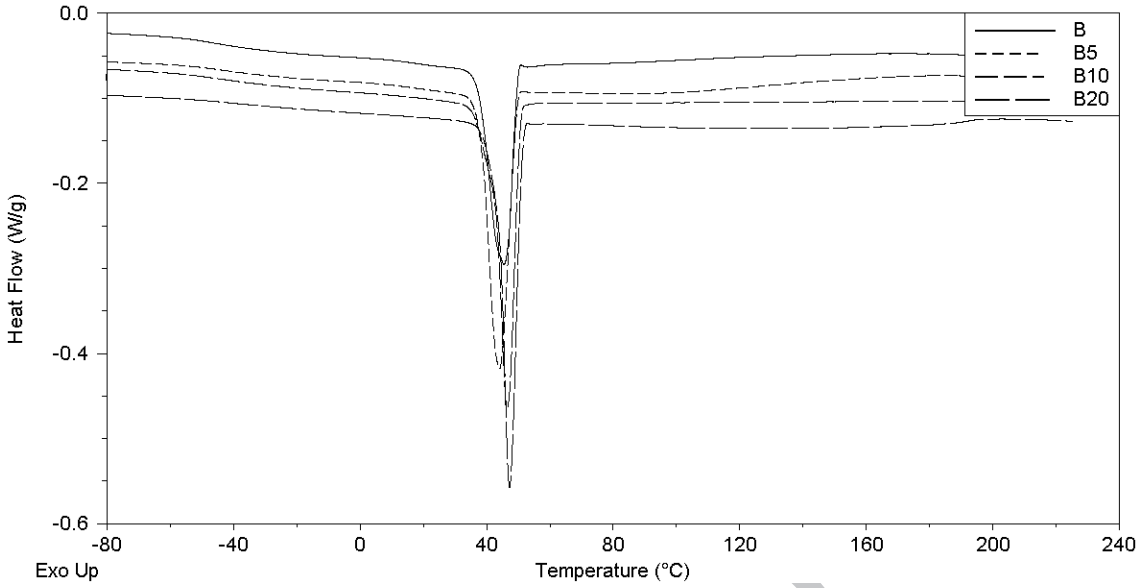


Figure 5

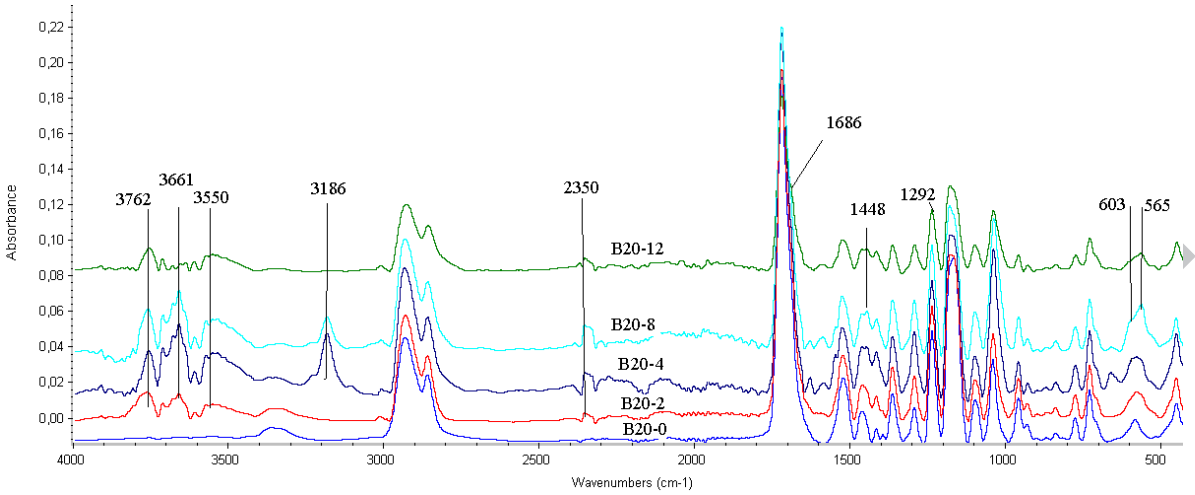


Figure 6

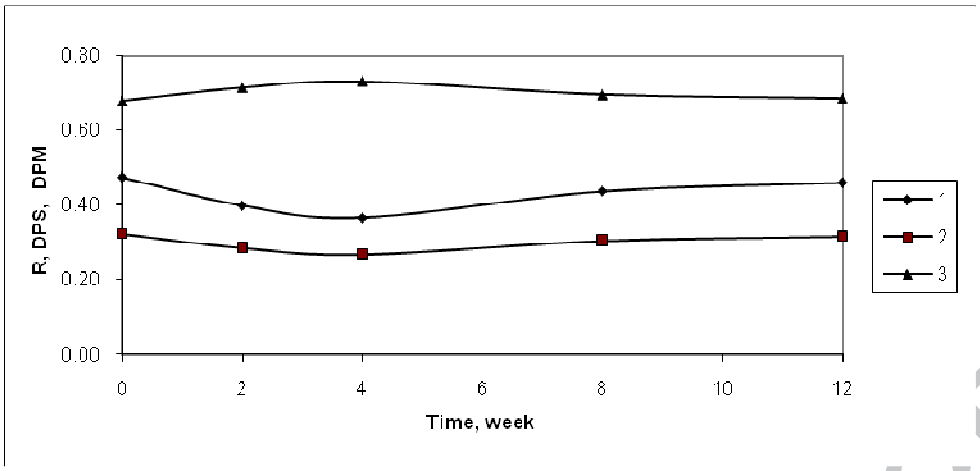


Figure 7

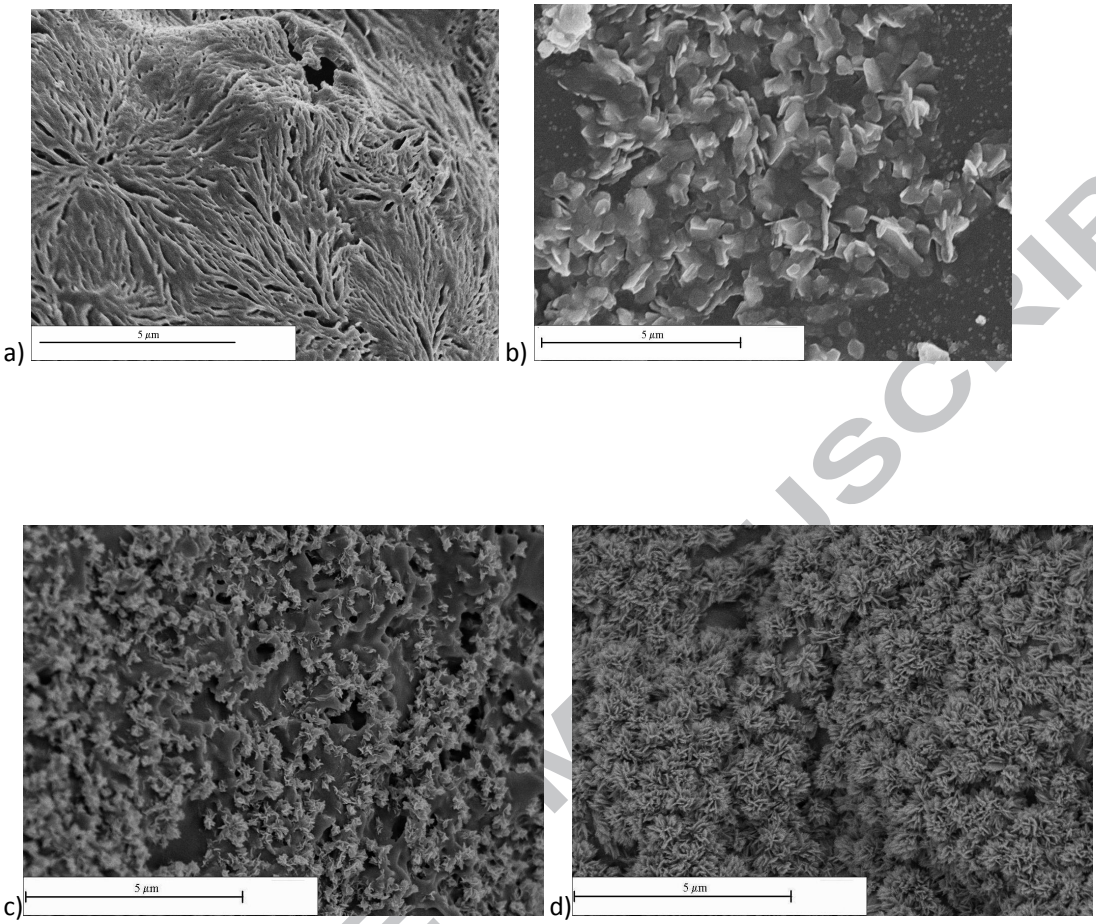


Figure 8

a) 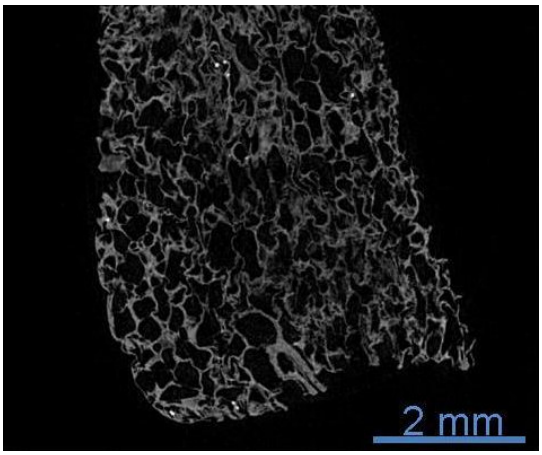


b) 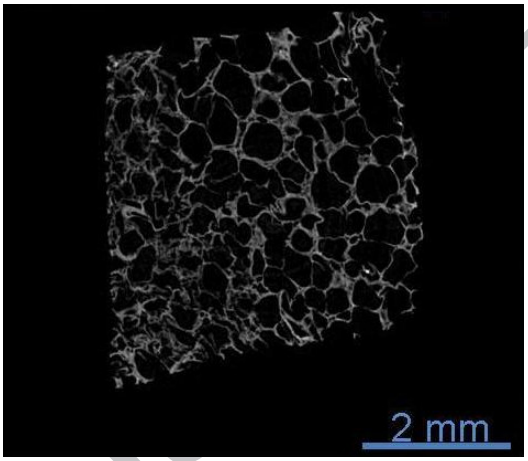


c) 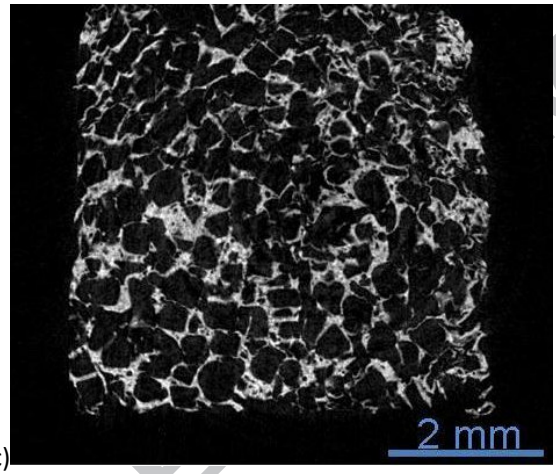


d) 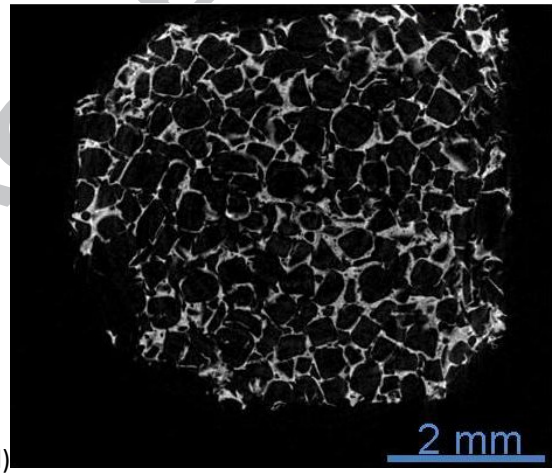

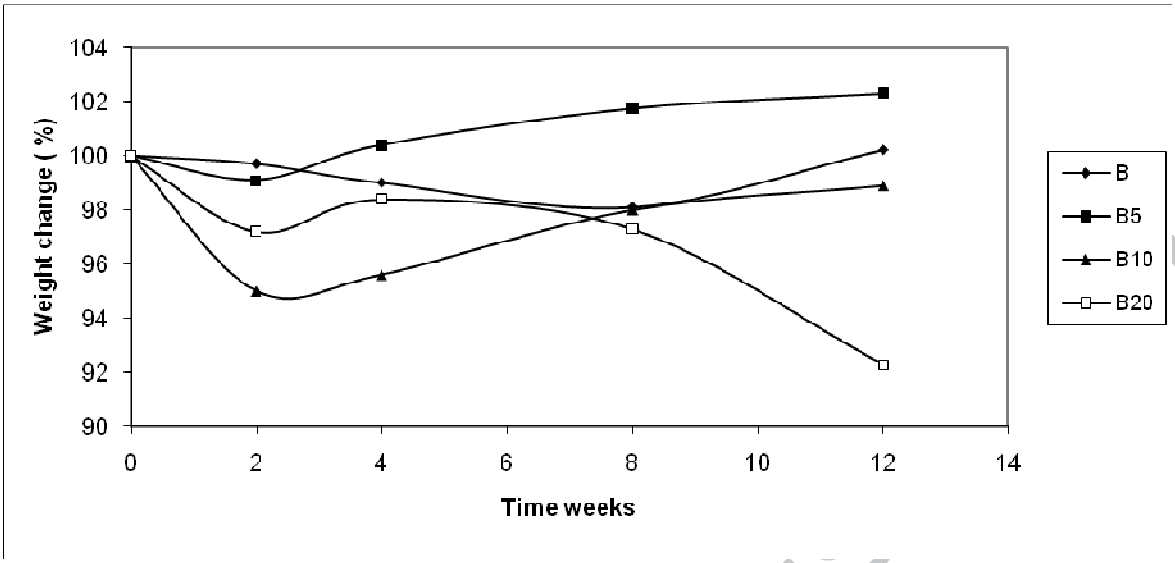


Figure 10

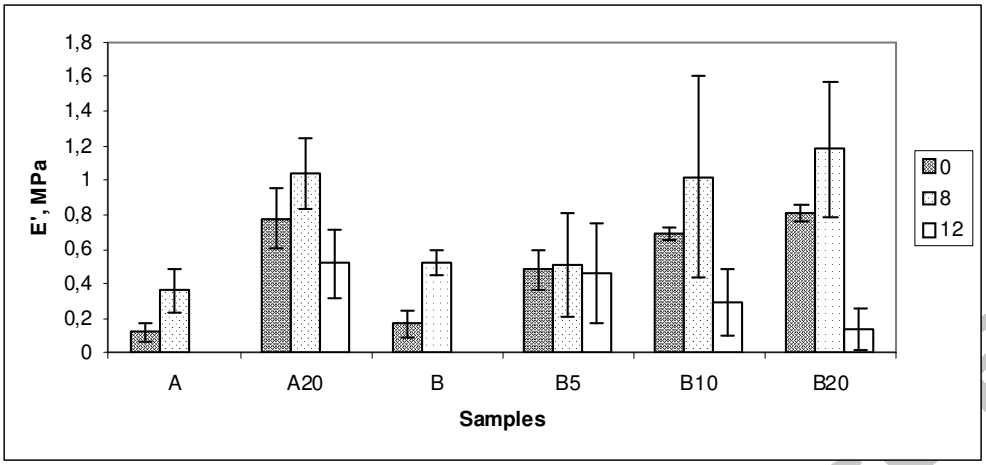


Figure 11

***Table 1. Properties of solid polyurethane and composites***

| Samples | A | B | C | A20 | B5 | B10 | B20 | C20 |
|---|---|---|---|---|---|---|---|---|
| α [°] | 75 | 71 | 75 | 69 | 72 | 67 | 69 | 74 |
| d [ g/cm3] | 1.14 | 1.05 | 1.11 | 1.24 | 1.13 | 1.17 | 1.26 | 1.15 |

Table 2. Polyurethane and composites pore size

| Sample | Average size of macropore [μm] | Size of micropore I interconnected [μm] | Average size of micropore II interconnected [μm] | Average size of all pores* [μm] |
|---|---|---|---|---|
| A | 340 | 50-90 | <10 | |
| A20 | 230 | 20-40 | <10 | 4.3 |
| B | 300 | 10-60 | <10 | 15.9 |
| B5 | 270 | 15-40 | <10 | 7.7 |
| B10 | 300 | 15-40 | <10 | 14.3 |
| B20 | 330 | 20-40 | <10 | 7.3 |

*measurement with Hg porosimeter ,

Table 3. Thermal analysis and DMA data

| Sample | Tg [˚C] | $Tg_1$ [˚C] | Tm [˚C] | $Tm_1$ [˚C] | ΔHm [J/g] | $ΔHm_1$ [J/g] | E' [MPa] | $E'_1$ [MPa] |
|---|---|---|---|---|---|---|---|---|
| A | -47.7 | -45.7 | 42.,8 | 42.9 | 42.9 | 46.9 | 0.12 | 0.36 |
| A20 | -46.5 | -44.6 | 49. 5 | 49.6 | 35.2 | 37.8 | 0.78 | 0.52 |
| B | -47.9 | -46.1 | 45.5 | 48.5 | 31.6 | 32.9 | 0.17 | 0.52 |

| | | | | | | | | |
|---|---|---|---|---|---|---|---|---|
| B5 | -45.2 | -42.0 | 44.1 | 49.4 | 35.5 | 35.2 | 0.48 | 0.46 |
| B10 | -41.,6 | -42.6 | 46.5 | 50.4 | 34.2 | 34.4 | 0.69 | 0.29 |
| B20 | -42.,0 | -34.9 | 47.2 | 51.7 | 34.3 | 39.6 | 0.81 | 0.14 |

Tg, $Tg_1$ - glass temperatures of porous materials before and after 12 weeks immersion in SBF, respectively

Tm, $Tm_1$ - melting temperatures of porous materials before and after 12 weeks immersion in SBF, respectively

$\Delta Hm$, $\Delta Hm_1$ – the enthalpy of fusion of soft segments of porous materials before and after 12 weeks immersion in SBF, respectively

E', $E'_1$ – storage modulus of porous materials at frequency 4.5Hz before and after 12 weeks immersion in SBF, respectively

Table 4. Porosity and pore size of neat polyurethane and composite foams measured by µCT

| Sample | Pt [%] | P [%] | $P_1$ [%] | D [µm] | $D_1$ [µm] | C [%] | $C_1$ [%] |
|---|---|---|---|---|---|---|---|
| A | 88.1 | 65.0 | 68.0 | | | | |
| A20 | 81.2 | 76.5 | 64.5 | 158 | 142 | 34 | 41 |

| | | | | | | | |
|---|---|---|---|---|---|---|---|
| B | 66.9 | 61.5 | 75.5 | 115 | 204 | 53 | 21 |
| B5 | 79.6 | 72.5 | 48.5 | 243 | 112 | 36 | 56 |
| B10 | 86.5 | 80.5 | 77.5 | 248 | 202 | 14 | 20 |
| B20 | 81.8 | 70.0 | 78.0 | 135 | 190 | 39 | 21 |

Pt- calculated total porosity

P, $P_1$- porosity of scaffolds before and after immersion in SBF, respectively

D, $D_1$- average pore size calculated as the diameter of the largest sphere which fits inside the pores, before and after immersion in SBF, respectively

C,$C_1$- percent of content of micropores with diameter <100µm before and after immersion in SBF, respectively

Table 5. TGA and DTA analysis data

| Sample | $T_1$ [˚C] | W1 [%] | $T_2$ [˚C] | W1 [%] | $T_3$ [˚C] | $T_4$ [˚C] | U [%] |
|---|---|---|---|---|---|---|---|
| B20 | 293 | 46 | 324 | 34 | - | - | 15.7 |
| B20_2 | - | | - | | 381 | 404 | 9.4 |
| B20_4 | - | | - | | 388 | 399 | 15.9 |
| B20_8 | - | | - | | 382 | 396 | 12.1 |
| B20_12 | - | | - | | 383 | - | 15.0 |

$T_1$ – temperature of the maximum weight loss rate of hard segments

$T_2$,$T_3$,$T_4$ – temperature of the maximum weight loss rate of soft segments

U – Char residue at 550°C